Transient Thin Film Laser Pyrolysis of RDX

Tod R. Botcher and Charles A. Wight*,†

Department of Chemistry, University of Utah, Salt Lake City, Utah 84112

Received: April 23, 1993; In Final Form: June 10, 1993

A new experimental technique is described for detecting initial pyrolysis products in rapidly heated condensed-phase energetic materials. A thin film sample is prepared by vapor deposition from a Knudsen oven onto a transparent substrate at 77 K. The film is heated to approximately 1000 K in 35 μs by irradiation with a pulsed CO_2 laser. The sample and initial reaction products are then quenched to 77 K on a millisecond time scale by conduction of heat into the substrate. Reaction products are identified by their characteristic transmission FTIR spectra obtained after laser pyrolysis. Detection of the NO_2 dimer molecule, N_2O_4, as an initial product in the thermal decomposition of condensed-phase RDX (hexahydro-1,3,5-trinitro-1,3,5-triazine) provides convincing evidence that the initial reaction step is homolysis of an N–N bond. No evidence is found for a competing concerted depolymerization pathway forming methylenenitramine, CH_2NNO_2.

Introduction

Cyclic nitramines such as 1,3,5-trinitro-1,3,5-triazine (RDX) and 1,3,5,7-tetranitro-1,3,5,7-tetrazine (HMX) are energetic materials that are used as propellants and explosives. Although many of the physical characteristics of explosions and detonations of these materials are well described by modern hydrodynamic theories of detonation,[1,2] mechanistic details of how chemical energy is released in these materials are only beginning to emerge.[3,4]

A search for the chemical mechanism of thermal pyrolysis in RDX and HMX has been the subject of several exerimental investigations[5-14] and computational studies.[15-17] Many of these studies suggest that N–N bond cleavage is the initial step in the reaction. Thermodynamic studies identify this as the weakest bond in the molecule,[18] and experimental studies on other nitramines provide indirect support for this mechanism.[2] However, a recent gas-phase molecular beam laser pyrolysis experiment[19] provides convincing evidence that a major decomposition route is the concerted depolymerization of gas-phase RDX to form three molecules of methylenenitramine, CH_2NNO_2. Pathways involving initial cleavage of an N–N bond account for only about one-third of the gas-phase product yield. A classical dynamics study recently published by Sewell and Thompson supports the viability of this depolymerization pathway.[20]

Perhaps the most detailed studies of thermal decomposition mechanisms in RDX and HMX have been carried out by Behrens and Bulusu using simultaneous thermogravimetric modulated beam mass spectrometry (STMBMS) measurements.[21-24] These authors have identified four major decomposition pathways for RDX, two of which exhibit first-order reaction kinetics (accounting for about 40% of the observed products) while the other two involve higher order reactions in their rate-limiting steps. Many of the products exhibit significant deuterium kinetic isotope effects, in agreement with earlier studies,[12,25] indicating that hydrogen-transfer reactions are rate-limiting in some of the pathways. In experiments of this type, samples are heated very slowly in comparison with the speed of product detection, so the temporal information reflects the rate-limiting steps in the reaction mechanism rather than the *initial* steps. Nevertheless, some information about initial steps can be inferred from the data. Interestingly, little evidence was found for the concerted depolymerization route, and only one of the channels was clearly identified as being initiated by N–N bond scission.

One of the important advances in this field has been the development of rapid heating and detection techniques for investigating early steps in the decomposition mechanisms. Brill and co-workers have developed rapid scan FTIR techniques for probing near-surface gas-phase decomposition products after subjecting samples to temperature jumps (2000 K/s) to a final burning temperature.[26,27] This group has also pioneered FTIR methodologies to measure the burn rates of propellants while monitoring simultaneous mass and temperature changes (SMATCH/FTIR).[28] These techniques probe reaction products under conditions that closely resemble realistic combustion conditions at pressures of 1 atm and higher.[29,30] These are crucial developments for determining combustion mechanisms under realistic conditions because the overall reaction kinetics and mechanistic pathways can be sensitive to the heating rates of molecules near the reaction zone.

A new experimental technique has been developed recently in our laboratory to detect *initial* products of thermal decomposition under realistic combustion conditions. This is accomplished by pulsed laser heating of a thin solid film of energetic material followed by thermal quenching of the film and FTIR detection of the trapped products. A brief report of our initial results was published recently.[31] In this paper, we present a more detailed account of the experimental procedure as well as more detailed and extended results for RDX pyrolysis.

Experimental Section

Apparatus. Samples are prepared in a vacuum Dewar cell illustrated schematically in Figure 1. This cell consists of a cold finger cooled with liquid nitrogen with an optical mount containing a 25-mm-diameter optical window (CsI, CaF_2, or sapphire) attached to the end. The cold finger is inserted into a rotatable vacuum shroud that is pumped to 10^{-5} Torr. Attached to one side of the shroud is a modified Knudsen oven described below. A quartz window mounted on the shroud opposite the oven permits us to monitor the film thickness by laser interferometry during deposition. A pair of CsI optical windows is mounted on the two remaining sides of the shroud for obtaining transmission IR spectra of the sample. During deposition, the shroud is turned so the cold optical window is normal to the path of the vaporized propellant coming from the oven. After deposition, the shroud is turned so the sample faces the two CsI windows. Spectra are obtained and pyrolyses are conducted in this configuration.

The deposition oven, shown schematically in Figure 2, is a machined block of OFHC copper with a 15-W button heater attached to one side and a chromel–alumel thermocouple for monitoring the temperature on the opposite side. The oven is housed in a small vacuum chamber which attached directly to

† Alfred P. Sloan Research Fellow, 1990–94.

0022-3654/93/2097-9149$04.00/0

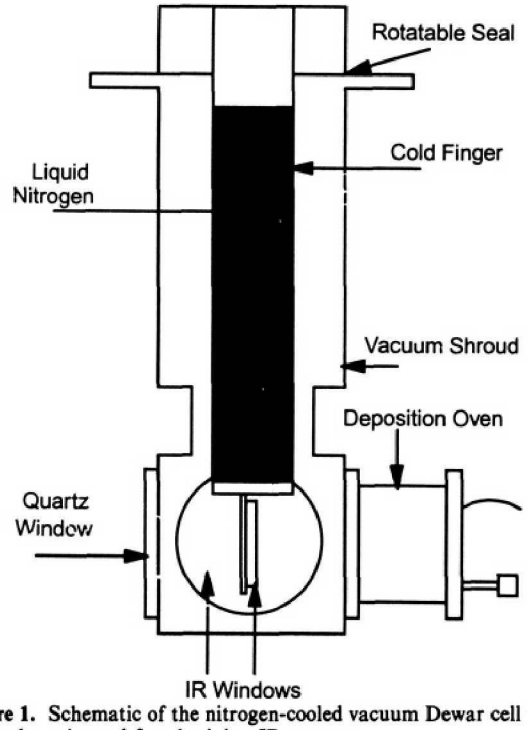

Figure 1. Schematic of the nitrogen-cooled vacuum Dewar cell viewed along the axis used for obtaining IR spectra.

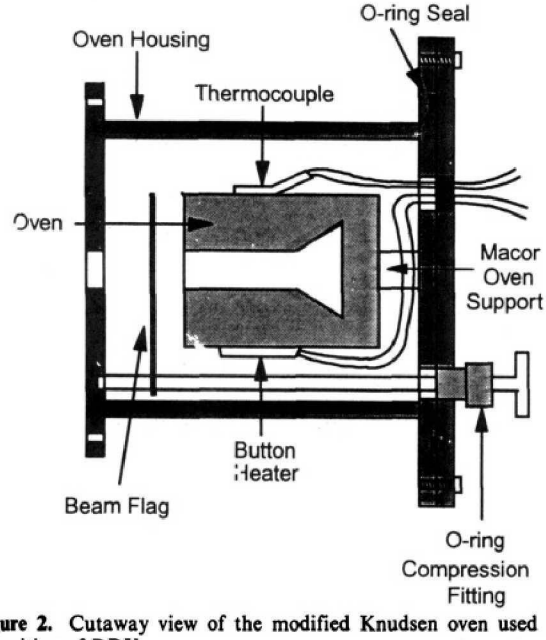

Figure 2. Cutaway view of the modified Knudsen oven used in the deposition of RDX.

the vacuum shroud. A small rotatable beam flag is manipulated by a rod which passes through an O-ring compression fitting. This flag can be moved to block the path of the propellant to the optical window, thereby controlling the deposition period. A modified oven incorporating a gas inlet is used for experiments requiring simultaneous deposition of gas-phase and solid-state reagents (e.g., NO_2 and RDX in this study). The modified oven is essentially the same as the one described above except that a gas deposition line is mounted just in front of the oven.

Infrared spectra are obtained with a Mattson Model Polaris FTIR spectrometer. Spectra are obtained by averaging 64 scans at 0.5-cm^{-1} resolution.

Pyrolysis of the samples is carried out with the use of a Pulse Systems Model LP140-G pulsed CO_2 laser tuned to the 10-μm P(20) line at 944 cm^{-1}. This laser has a nominal pulse length of 35 μs and is used at a repetition rate of 1 pulse/s.

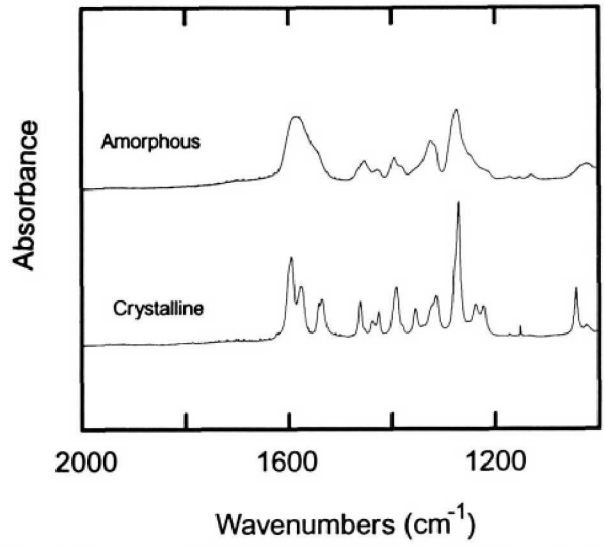

Figure 3. Two spectra illustrating the phase change of RDX upon heating. The top spectrum is of an amorphous sample created by vapor deposition. The bottom spectrum is of the same sample after heating to room temperature and recooling to 77 K (no second window was used). The narrowing of the bands is typical of a disorder to order transition.

Interferometry Experiments. The thickness of RDX samples is monitored by laser interferometry during deposition from the Knudsen oven onto a sapphire window at 77 K. The intensity of a He–Ne laser beam reflected from the substrate (9° incident angle with respect to the surface normal) is monitored during deposition of the sample (oven temperature is 120 °C; substrate temperature is 77 K). The shutter mounted in front of the oven is used to control the start and stop of the deposition process. Fringes (oscillations in the reflected intensity with increasing sample thickness during deposition) are caused by interference between reflections from the sample/substrate interface and those from the sample/vacuum interface during growth of the sample. The thickness of the sample is given by

$$d = \frac{m\lambda_0}{2n \cos \theta_r} \quad (1)$$

where m is the number of interference fringes, n is the refractive index of the film, and θ_r is the angle of refraction of the light inside the film (calculated by Snell's law). Infrared spectra are obtained of RDX samples of measured thickness, so the thickness of subsequent samples is determined on the basis of IR absorption cross sections. In the pyrolysis experiments, the samples are approximately 20 mm in diameter by 13 μm thick.

Pyrolysis Experiments. Four types of pyrolysis experiments are conducted. In the first "double-window" type, a film of RDX is formed by vapor deposition from the Knudsen oven onto the substrate window (CaF_2 or CsI). The thin film is then warmed to room temperature to allow conversion from the amorphous to a crystalline state (Figure 3). This procedure is necessitated by the fact that laser pyrolysis causes amorphous samples to partially crystallize, leading to significant changes in positions and widths of IR absorption bands of RDX which could mask product absorptions. A second window is then placed over the sample, and the "sandwich" arrangement is remounted in the vacuum Dewar vessel and recooled to 77 K. The entire sample is then subjected to a single low-fluence pulse from the CO_2 laser (typically 0.3 J cm^{-2}). FTIR spectra are obtained before and after the laser pyrolysis to record any physical or chemical changes in the sample. This cycle of laser pyrolysis and infrared spectroscopy is repeated on the same sample at successively higher laser fluence (to about 4.7 J cm^{-2}). The spectra are then analyzed to determine the fluence at which product formation is first detected. High-fluence pyrolysis runs are conducted by reducing the beam size with a concave gold mirror (1-m focal length) and

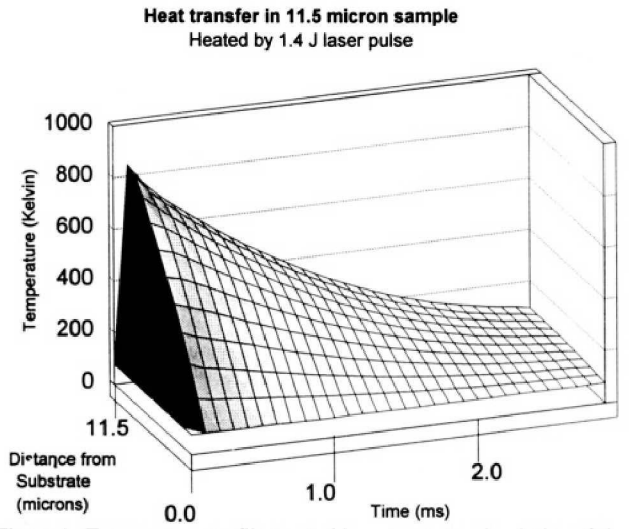

Figure 4. Temperature profile created by a computer simulation of the pyrolysis experiments. The film of RDX was heated from the vacuum side and allowed to cool for 2.9 ms. Greater degrees of shading indicate a greater change from neighboring data points in the vertical dimension.

rastering the beam across the sample such that each area of the sample is subjected to a single laser pulse. The rastering process is monitored by placing thermal paper behind the sample cell and adjusting the position of the beam between pulses such that the paper is uniformly developed. The beam from this laser is approximately square in shape, making it relatively easy to obtain uniform illumination of the sample. The purpose of installing the second window in these experiments is to ensure the condensation and trapping of all reaction products formed in the laser pyrolysis.

The second type of experiment is a double-window experiment similar to that described above, except that samples are pyrolyzed several times at the same laser fluence. The third type of experiment is conducted on a "single-window" crystalline sample prepared in the same way as above except that it is left uncovered. Reaction products that are formed at temperatures higher enough to vaporize the films are lost from the substrate window in these experiments.

The fourth type of experiment is similar to the "single-window" experiment just described except that no annealing cycle is performed; the sample is left in its amorphous state.

All pyrolysis experiments are conducted using the 10-μm P(20) line of a pulsed CO_2 laser at 944 cm^{-1}. This heats the sample from 77 K to approximately 1000 K in 35 μs (the nominal pulse width of the laser). Because the films are thin and in contact with a relatively massive substrate at 77 K, the products and unreacted propellant are cooled with a characteristic time constant estimated to be 0.001–0.004 s. This estimate is based on a computer simulation in which the one-dimensional heat diffusion equation is solved during the laser heating and conductive cooling cycles. This simulation assumes that the thermal conductivity of the RDX is independent of temperature. The temperature dependence of the heat capacity is estimated by the procedure described in the next section. The substrate (CsI) is assumed to have a constant 77 K temperature and a thermal conductivity large compared to the sample. The output of the simulation is the sample temperature as a function of time and distance from the substrate window. Representative results are shown in Figure 4.

The experimental conditions create a large temperature gradient within the thin film due to the fact that both the heating and cooling rates are functions of distance from the substrate. It is reasonable to assume that the spatial distributions of products and unreacted RDX molecules are highly nonuniform; the zone of highest product concentration lies near the vacuum interface where cooling is least efficient. Although the technique is well

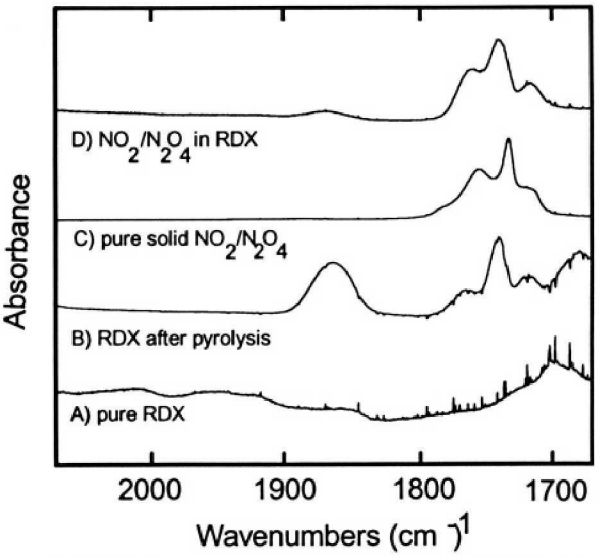

Figure 5. (A) 1-h deposition from 120 °C oven onto 77 K CsI window. Sample was warmed to room temperature, covered with a second CsI window, and cooled to 77 K. (B) Same RDX sample after rastering with 4.7 J/cm^2-pulse 10-μm P(20) line of a CO_2 laser. (C) 1.9 Torr of NO_2 deposited onto a 77 K CsI window. (D) 2.4 Torr of NO_2 codeposited with RDX from a 120 °C oven onto a 77 K CsI window.

suited to determining the identity of initial reaction products, it is not practial to obtaining quantitative product concentrations or rate constants.

Calculation of Internal Energies of RDX. The internal energy of RDX is calculated as a function of temperature using the formula

$$\langle E_{vib} \rangle = \sum_v \frac{Nk\Theta_v}{\exp(\Theta_v/T - 1)} \quad (2)$$

where

$$\Theta_v = h\nu/k \quad (3)$$

and ν is the vibrational frequency of each normal mode. Most of the normal mode frequencies of RDX are taken from the results of Sewell and Thompson.[20] The frequencies of the six remaining internal vibrational modes and six phonon/libron modes are lumped as a single frequency (i.e., an Einstein model) which is adjusted to give the correct heat capacity for RDX at room temperature (C_p = 1.126 J/(g-K)).[32] The heat capacities are calculated from the derivative of eq 2 and fit to a third-order polynomial in T for use in the computer simulations.

Results

Twelve separate experiments were conducted on crystalline RDX samples in the "double-window" configuration. Laser pyrolysis at laser fluence lower than 1.4 J cm^{-2} results in slight changes in the infrared band shapes of RDX due to structural changes. When laser pulses at or slightly above 1.4 J cm^{-2} are used, a new absorption feature appears at 1736 cm^{-1}. This band is assigned as N_2O_4 (the nitric oxide dimer molecule) based on good agreement with previous assignments of the N_2O_4 infrared spectrum in the literature by Smith and Guillory[33] and by Hisatsune.[34] The shape and position of this product band are also in excellent agreement with a band observed at 1735 cm^{-1} after deposition of a thin film of pure NO_2/N_2O_4 in our apparatus. Representative spectra of this region are presented in Figure 5.

The integrated intensity of the N_2O_4 product band observed at 1.4 J cm^{-2} fluence reveals that the extent of RDX decomposition under these conditions is slight. Only 1.3 × 10^{-3} mol of N_2O_4 is produced per mole of RDX in the sample. The RDX band intensities remain unchanged within experimental uncertainty (approximately 3% due to the aforementioned structural changes).

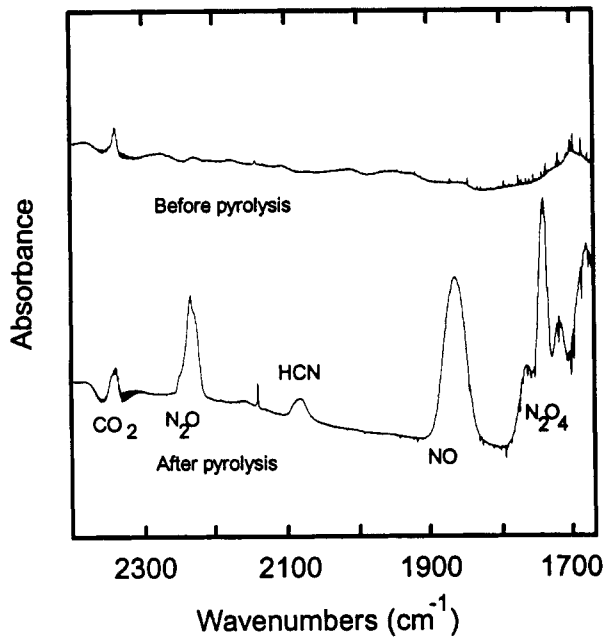

Figure 6. Spectra of RDX before and after pyrolysis at 4.7 J/cm². Note the abundance of secondary products in the sample.

TABLE I: Product Band Intensities for RDX Pyrolysis at 3.5 J/cm²

	relative intensities[a]			
band (cm^{-1})	double-window Xtal	single-window Xtal	single-window amorphous	assign.
1736	0.661	0.163	0.176	N_2O_4
1864	0.232	0.018	0.015	NO
2086	0.012	0.010	0.040	HCN
2236	0.114	0.004	0.018	N_2O
2343	0.024	0.0017	0.013	CO_2

[a] Values given are ratios of integrated band intensity for the band centered at the given value to the integrated band intensity of the RDX band located at 3050 cm^{-1} in its amorphous form.

At 3.5 J cm^{-2}, other product bands are observed. These include features at 1864 cm^{-1} (NO), 2086 cm^{-1} (HCN), 2236 cm^{-1} (N_2O), and 2343 cm^{-1} (CO_2), along with the N_2O_4 band centered at 1736 cm^{-1} (Figure 6). The relative integrated intensities of product bands are given in Table I. Other products which are formed in the decomposition are not observed due to spectral interference with RDX bands. Under these conditions, the RDX bands indicate a loss of approximately 8.5% of the reactant. The corresponding amount of N_2O_4 produced is consistent with loss of a single NO_2 monomer from each RDX molecule.

The same products are observed in constant-high-fluence double-window experiments conducted at 4.7 J cm^{-2}. Approximately 20% of the RDX reacts after one pulse at 4.7 J cm^{-2}, based on measured decreases in the integrated intensities of RDX absorption bands.

Nine experiments were conducted on crystalline RDX in the single-window configuration. In low-fluence experiments (1.4 J cm^{-2}) that utilized a CsI substrate, a band appears at 1738 cm^{-1} (N_2O_4) that is similar in shape and integrated intensity to the N_2O_4 band observed in the double-window experiments described above. A similar single-window experiment on CaF_2 exhibits essentially the same results with no evidence for other product bands. From this result, we can reasonably conclude that the nature of the substrate does not affect the mechanism or threshold for formation of initial products. In addition, we know that the N_2O_4 is formed in the condensed phase, because if reactions take place in the gas phase (above the sample surface), a substantial loss of product from the sample window is expected.

The results of high-fluence single-window experiments on crystalline samples can be compared with those of comparable double-window experiments in order to assess the relative importance of secondary product formation in the gas phase versus condensed phase. It should be noted that in the high-fluence single-window experiments as much as 75% of the sample is lost to vaporization. To make the comparison, we have listed the relative integrated band intensities of the various products formed at 3.5 J cm^{-2} in Table I. In order to correct for slight differences in overall sample size, the raw integrated intensities have been divided by the integrated intensity of one of the parent RDX bands in its amorphous form prior to thermal annealing or laser pyrolysis. Although the same product bands appear in both types of experiments, the smaller values for the single-window experiments reflect the amount of sample lost to vaporization at high fluence. Variations in the relative intensities of the various products provide qualitative information about whether or not each product is formed primarily in the condensed phase or in the gas phase.

Four experiments were conducted on amorphous samples. The purpose of these experiments was to test whether the introduction of spatial and orientational disorder changes the product yield. The reasoning is that if bimolecular reactions play a significant role in the initial decomposition, then the distributions of orientations associated with the amorphous form should have a significant effect on the rate of thermal decomposition. A direct comparison of single-window experiments on amorphous and crystalline samples (Table I) shows that the yields of N_2O_4 are essentially the same, though there are small differences in the yields of the other (secondary) products.

In several experiments, thin films of NO_2 were prepared for comparison to the postpyrolysis spectra of RDX. Samples of pure NO_2 as well as NO_2 codeposited with RDX were prepared and the IR spectra obtained. A small amount of NO_2/N_2O_4 (0.2 mol) was released into a vacuum manifold and allowed to equilibrate for 15 min. A thin film was formed by vapor depositing 0.035 mol onto a CsI window at 77 K, and an FTIR spectrum was obtained.

For codeposited samples, the NO_2/N_2O_4 was released into a manifold and allowed to equilibrate while the oven heated. The RDX and the gas mixture were codeposited through a Knudsen cell oven at 120 °C which had been modified to allow a dual deposition. The deposition occurred over a 20-min period with 0.045 mol of the NO_2/N_2O_4 being deposited in the RDX onto a 77 K CsI window.

In none of these experiments was there any evidence for the presence of CH_2NNO_2. Although the infrared spectrum of this molecule is not known, its vibrational frequencies have been calculated by Mowry *et al.*[35] Many of the bands expected for this molecule lie in regions which are obscured by the absorptions of RDX. However, three bands at 1220, 896, and 621 cm^{-1} lie in regions which are relatively free of interference from RDX and should be easily observable by spectral subtraction techniques (see Table II). These bands were never observed in the pyrolysis experiments.

Discussion

Our experimental results lead us to believe that N–N bond scission is the dominant initial step in the solid-state thermal decomposition of RDX. The only product observed in the low-fluence single-window crystalline sample experiments (which trap only solid-state reaction products) is the N_2O_4. The double-window experiments initially show the presence of the N_2O_4 band; secondary products (NO, CO_2, N_2O, and HCN) appear after more intense heating by higher fluence laser pulses. The secondary products appear in both the single- and double-window high-fluence experiments but with somewhat differing ratios.

From this, we conclude two things. First, N_2O_4 is an *initial* reaction product in the solid state. The other products are formed

TABLE II: Band Positions for Methylenenitramine

calcd position for CH_2NNO_2[a]	obsd in postpyrolysis spectra
3482.6	broad feature
3360.6	broad feature
1839.0	assigned to NO
1611.9	obscured by RDX
1580.0	obscured by RDX
1310.6	obscured by RDX
1261.2	obscured by RDX
871.9	obscured by RDX
665.1	obscured by RDX
560.6	obscured by RDX
1229.4	not present
895.7	not present
620.8	not present

[a] From ref 35.

via subsequent reactions in the overall decomposition mechanism. Second, the subsequent decomposition takes place at least partly in the gas phase. To be precise, these reactions occur only under conditions where a large fraction of the RDX is vaporized from the substrate.

We were surprised to observe significant yields of N_2O_4 as an initial product when no NO_2 monomers were apparent in the spectrum (though the spectral region where NO_2 absorptions are expected is heavily congested with RDX bands). Observation of the dimer raised the possibility that bimolecular encounters of neighboring RDX molecules might be important in the initial steps of the thermal decomposition mechanism. However, experiments conducted on single-window amorphous and crystalline samples gave virtually identical yields of N_2O_4. It is reasonable to assume that if bimolecular encounters were important in the mechanism, the orientational disorder present in the amorphous samples would have a significant effect on the yield of N_2O_4. The extent of sample crystallization in these experiments is slight (as evidenced by slight narrowing of the parent RDX infrared bands). This is because the length of time the sample is heated is too short for extensive crystallization to occur. The experimental evidence therefore clearly implicates unimolecular scission of the N–N bond in RDX as the initial step in the decomposition mechanism.

It is also somewhat surprising that we find little evidence for products containing carbon and hydrogen, especially CH_2O, which is not formed in detectable quantities under our experimental conditions. We speculate that most of the carbon may remain as relatively large organic fragments (which are masked by RDX absorption bands in our experiment) until relatively late in the reaction sequence.

Our results may seem to be in conflict with those obtained by Zhao *et al.* for laser pyrolysis of gas-phase RDX molecules in a molecular beam.[19] However, the two experiments are carried out under drastically different conditions. Our experiments were done in the condensed phase, while their experiment was done in the gas phase. Although we observe only N_2O_4, our results strongly suggest that the initial decomposition of each RDX molecule releases a single NO_2 molecule. The second NO_2 could come from a second RDX molecule or be removed from the same RDX molecule at a later point in the decomposition. In the gas phase, the RDX decomposes preferentially to three molecules of methylenenitramine. The difference between the two reaction pathways is that in the solid state the molecule is restricted to a relatively small volume, while in the gas phase there is no such limitation. The concerted depolymerization has a large volume of activation, and this causes the N–N bond scission mechanism to dominate in the solid state.

Acknowledgment. We thank Dr. Robert Fifer for generously supplying the RDX samples. This research is supported by the U.S. Army Research Office under Contract No. DAAL03-90-G-0043.

References and Notes

(1) Meyer, R. *Explosives*; Verlag Chemie: Weinkeim, 1977.
(2) Federoff, B. T.; Sheffield, O. E. *Encyclopedia of Explosives and Related Items*; Picatinny Arsenal: Dover, NJ, 1966; Rpt. No. PATR-2700, Vol. III.
(3) Adams, G. F.; Shaw, Jr., R. W. *Annu. Rev. Phys. Chem.* **1992**, *43*, press.
(4) Alexander, M. H.; Dagdigian, P. J.; Jacox, M. E.; Kolb, C. E.; Melius, C. F. *Prog. Energy Combust. Sci.* **1992**, *54*, 203.
(5) Brill, T. B.; Brush, P. J. *Phil. Trans. R. Soc. London* A **1992**, *339*, 377.
(6) Brill, T. B. In *Chemistry and Physics of Energetic Materials*; Bulusu, S. N., Ed.; Kluwer: London, 1990.
(7) Brill, T. B.; Karpowicz, R. J. *J. Phys. Chem.* **1982**, *86*, 4260.
(8) Karpowicz, R. J.; Brill, T. B. *J. Phys. Chem.* **1984**, *88*, 348.
(9) Oyumi, Y.; Brill, T. B. *Combust. Flame* **1977**, *62*, 233.
(10) Mesaros, D. V.; Oyumi, Y.; Brill, T. B.; Dybowski, C. *J. Phys. Chem.* **1986**, *90*, 1970.
(11) Oxley, J. C.; Hiskey, M.; Naud, D.; Szekeres, R. *J. Phys. Chem.* **1992**, *96*, 2505.
(12) Bulusu, S.; Weinstein, D. I.; Autera, J. R.; Velicky, R. W. *J. Phys. Chem.* **1986**, *90*, 4121.
(13) Suryanarayana, B.; Graybush, R. J.; Autera, J. R. *Chem. Ind.* **1967**, 2177.
(14) Suryanarayanan, K.; Bulusu, S. *J. Phys. Chem.* **1972**, *76*, 496.
(15) Habibollahzadeh, D.; Grodzicki, M.; Seminario, J. M.; Politzer, P. *J. Phys. Chem.* **1991**, *95*, 7699.
(16) Wallis, E. P.; Thompson, D. L. *Chem. Phys. Lett.* **1992**, *189*, 363.
(17) Cohen, N. S.; Lo, G. A.; Crowley, J. C. *AIAA Journal* **1985**, *23*, 276.
(18) Melius, C. F. In *Chemistry and Physics of Energetic Materials*; Bulusu, S. N., Ed.; Kluwer: London, 1990.
(19) Zhao, X.; Hintsa, E. J.; Lee, Y. T. *J. Chem. Phys.* **1988**, *88*, 801.
(20) Sewell, T. D.; Thompson, D. L. *J. Phys. Chem.* **1991**, *95*, 6228.
(21) Behrens, Jr., R. *J. Phys. Chem.* **1990**, *94*, 6706.
(22) Behrens, Jr., R.; Bulusu, S. *J. Phys. Chem.* **1991**, *95*, 5838.
(23) Behrens, Jr., R.; Bulusu, S. *J. Phys. Chem.* **1992**, *96*, 8877.
(24) Behrens, Jr., R.; Bulusu, S. *J. Phys. Chem.* **1992**, *96*, 8891.
(25) Rodgers, S. L.; Coolidge, M. B.; Lauderdale, W. J.; Shackleford, S. A. *Thermochim. Acta* **1991**, *177*, 151.
(26) Brill, T. B. *Anal. Chem.* **1989**, *61*, 897A.
(27) Brill, T. B.; Brush, P. J.; James, K. J.; Shepherd, J. E.; Pfeiffer, K. J. *Appl. Spectrosc.* **1992**, *46*, 900.
(28) Timken, M. D.; Chen, J. K.; Brill, T. B. *Appl. Spectrosc.* **1990**, *44*, 703.
(29) Palopoli, S. F.; Brill, T. B. *Combust. Flame* **1991**, *87*, 45.
(30) Brill, T. B.; Brush, P. J.; Kinloch, S. A.; Gray, P. *Phil. Trans. R. Soc. London Ser. A* **1992**, *339*, 377.
(31) Wight, C. A.; Botcher, T. R. *J. Am. Chem. Soc.* **1992**, *114*, 8303.
(32) Dobratz, B. M. *Properties of Chemical Explosives and Explosive Simulants*; Lawrence Livermore Laboratory: Livermore, CA, March 1981; Rept. No. UCRL-52997, pp 19–132.
(33) Smith, G. R.; Guillory, W. A. *J. Mol. Spectrosc.* **1977**, *68*, 223.
(34) Hisatsune, I. C. In *Advances in Molecular Spectroscopy*, Mangini, A., Ed.; Pergamon Press: New York, 1962.
(35) Mowry, R. C.; Page, M.; Adams, G. F.; Lengsfeld, III, B. H. *J. Chem. Phys.* **1990**, *93*, 1857.